Proceedings of ASME Turbo Expo 2011
GT2011
June 6-10, 2011, Vancouver, British Columbia, Canada

GT2011-46031

HEAT TRANSFER ENHANCEMENT IN A RECTANGULAR CHANNEL WITH THE COMBINATION OF RIBS, DIMPLES AND PROTRUSIONS

Jibing Lan, Yonghui Xie, Di Zhang
Xi'an Jiaotong University
School of Energy and Power Engineering
Xi'an, Shaanxi Province, 710049, P. R. China
Tel: 86-29-82664443, Fax: 86-29-82664443

ABSTRACT

Rib turbulators can enhance the heat transfer successfully, but in most cases this is associated with large pressure loss penalties. Recently, dimple techniques become an attractive method for gas turbine blade internal cooling because dimples enhance heat transfer with low pressure penalty. In the present paper, a compound heat transfer enhancement technique, heat transfer enhancement in rectangular channel (Aspect ratio = 4) with the combination of ribs, dimples and protrusions, are investigated. The calculations are conducted on five different channel configurations. Case 1 which is the baseline configuration is a rectangular channel with rectangular ribs (e/D_h=0.078, P/e=10). In case 2, one row of dimples are placed between two ribs. In case 3, instead of dimples, one row of protrusions are placed between two ribs. In case 4, three rows of dimples are place between two ribs. Case 5 places three rows of protrusions between two ribs instead of dimples. The present paper focuses on Reynolds numbers (based on the channel hydraulic diameter) ranging from 10000 to 60000. In all configurations, the non-dimensional dimple/protrusion depths are 0.2. The results show that the rib+dimple cases provide minor increase in Nu/Nu_0, f/f_0 and thermal performance. Within the Reynolds number range studied, the Nu/Nu_0 values of the three row rib+protrusion case is 17% ~ 7% higher than that of the baseline case, and the decrease in f/f_0 is about 10%. The thermal performance of the three row rib+protrusion case is about 16% higher than that of the baseline case. The Nu/Nu_0 values of the one row rib+protrusion case is about 9% higher than that of the baseline case, and the decrease in f/f_0 is about 12%. The thermal performance of the one row rib+protrusion case is about 14% higher than that of the baseline case. It can be concluded that rib+protrusion technique in rectangular channel has the potential to provide heat transfer enhancement with low pressure penalty.

Keywords: Heat transfer enhancement; dimple; rib; protrusion; gas turbine.

INTRODUCTION

The increasing demand for highly efficient gas turbines requires the gas turbine cycle to operate at extremely high temperatures. Therefore, several gas turbine components are exposed to temperatures which exceed the maximum allowable temperature of the material. The installation of rib turbulators is the most common method used to enhance the heat transfer on the coolant passage walls. Han and his co-workers[1-7] have made a large amount of research in this area, and when it comes to correlations of this kind, it is difficult to find articles that he has not been involved in. Rib turbulators can enhance the heat transfer successfully, but in most cases this is associated with large pressure loss penalties. As reviewed by Ligrani [8], friction factor ratios can be as high as 71 for channels with rib turbulators.

Dimple technique becomes an attractive method for heat transfer enhancement because dimples enhance heat transfer with low pressure penalty. One of the early investigations was conducted by Afanasyev [9], who investigated the effect of applying shallow dimples on flat plates on the overall heat transfer and pressure drop for turbulent flow. Moon [10] studied the effect of channel height, and presented that the improvement on heat transfer is insensitive to channel height when its value is greater than dimple depth. Ligrani [11] reported instantaneous, dynamic and time-averaged characteristics of the vortex structures of a channel with one dimpled wall. Mahmood [12] studied the flow and heat transfer characteristics over a set of staggered dimple arrays. The effects of inlet stagnation temperature, channel height,

and Reynolds number were investigated. Ligrani [13] studied the effect of the combined effect of dimples and protrusions on the opposite wall and showed that protrusions increase heat transfer and friction coefficients by means of increased mixing and vortex stretching. Won [14] experimentally studied the flow structural characteristics over dimple surfaces located on one wall of a rectangular channel with three different dimple depths (δ/D=0.1, 0.2, and 0.3). Burgess [15] developed empirical correlations for relative Nusselt numbers and friction factors as a function of *δ/D* in the Reynolds number range from 5000 to 80000. The correlations showed good agreement with previously published experimental data. Ligrani [16] studied the effect of the inlet turbulence level on the heat transfer improvement in walls with dimples of *δ/D* =0.1, showing that as the turbulence level is increased the relative Nusselt number is reduced. Experimental work on dimple applications for microchip cooling was presented by Small [17]. Xiao [18] provided data which illustrated the effects of an array of dimples on local and spatially averaged surface Nusselt number distributions, as well as on friction factors in channels with laminar flow.

Numerical study of flow and heat transfer characteristics of dimples was conducted by a number of researchers. Isaev [19] analyzed the three-dimensional steady-state vortex structures around a deep spherical dimple on a plane by using a factorized finite volume method to solve the Navier–Stokes equations. Park [20] used Fluent to solve the steady state Reynolds Averaged Navier-Stokes (RANS) equations to study flow and heat transfer in dimpled channel in the turbulent regime. Wang [21] used Direct Numerical Simulation (DNS) to study turbulent flows over dimpled surfaces in a channel. Wei [22] studied the steady, laminar flow and heat transfer, inside a rectangular microchannel with dimpled bottom surface numerically. Elyyan [23, 24] used Large Eddy Simulation (LES) to investigate the heat transfer and friction in a channel with dimples and protrusions on either side.

Dimpled surfaces provide enhancement in heat transfer by about 1.5-3.0 times and friction factor of 1.6–4.0 times that of smooth channel. In the present paper, a compound heat transfer enhancement technique, heat transfer enhancement in rectangular channel (AR = 4) with the combination of ribs, dimples and protrusions, are investigated. Flow characteristics, heat transfer performances and friction factor characteristics are obtained.

NUMERICAL METHOD

Computational Geometry

A schematic diagram of the rib roughened rectangular channel used in this study is shown in Fig. 1. The coordinates *x*, *y*, *z* represent the streamwise, normalwise, and spanwise direction, respectively. All the parameters is the same with that of Rectangular Channel II in Han[3]. The rectangular channel is 102 mm (*W*) × 25.5 mm (*H*) in cross-section. The channel is roughened with square ribs (*a*/*e* = 1) on two larger opposite walls in an in-line arrangement. The block ratio (e/D_h) is 0.078, and the height normalized pitch (*P*/*e*) is 10. The placement of the ribs is orthogonal to the flow direction. Fig. 2 shows the cross-sectional details of the dimple and protrusion used in the present paper.

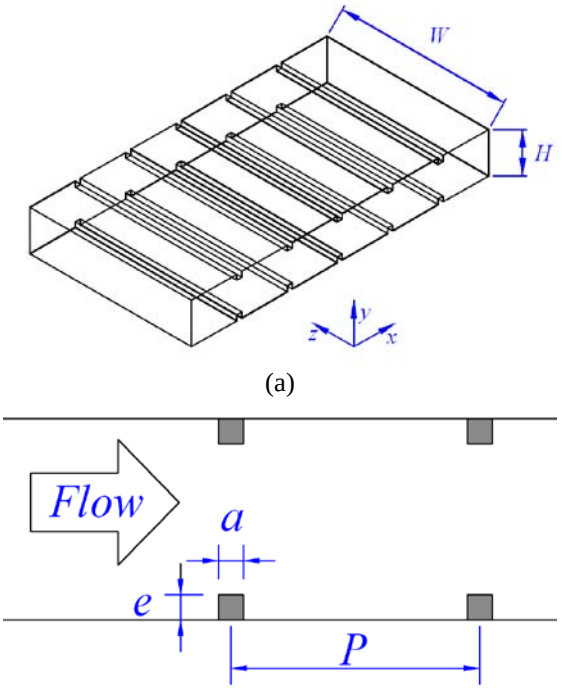

Fig. 1 Schematic diagram of the rib roughened channel: (a) rectangular channel with a pair of opposite ribbed walls; (b) geometry of the ribs

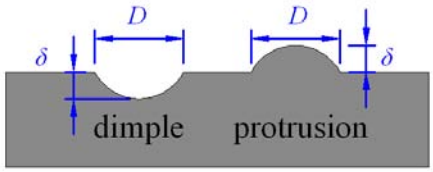

Fig. 2 Cross-sectional view of the dimple/protrusion

Five different configurations are employed in the present study. Case 1 is the baseline case without dimples and protrusions. In case 2, one row of dimples are placed between two ribs, and the arrangement is shown in Fig. 3 (a). In case 3, instead of dimples, one row of protrusions are placed between two ribs, the arrangement is the same to that of case 2. In case 4, three rows of dimples are place between two ribs, the arrangement is shown in Fig. 3(b). Case 5 places three rows of protrusions between two ribs instead of dimples, the protrusion arrangement is the same to that of case 4. The detailed parameters are presented in Table 1.

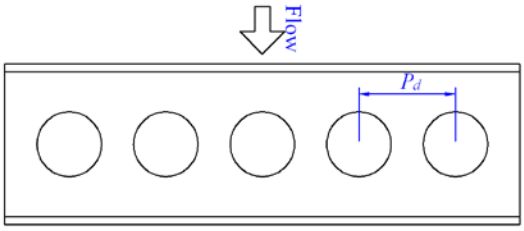

(a)

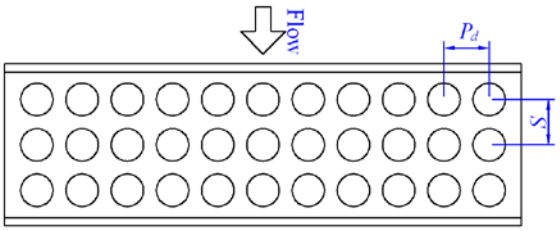

(b)

Fig. 3 Top view of the dimple/protrusion arrangement:(a) case 2 and 3; (b) case 4 and 5

Table 1 Parameters of the cases

	Type	δ/D	D/D_h	P_d/D	S/D
case 1	rib	—	—	—	—
case 2	rib+dimple	0.2	0.313	1.5	—
case 3	rib+protrusion	0.2	0.313	1.5	—
case 4	rib+dimple	0.2	0.165	1.4	1.4
case 5	rib+protrusion	0.2	0.165	1.4	1.4

Solution Method

The Navier-Stokes equation in its steady form is solved using the finite-volume based computational fluid dynamics solver FLUENT. The SIMPLEC algorithm is used to solve the pressure-velocity coupling. The standard scheme is used for pressure discretization. The momentum and energy equations are solved with second-order up-wind scheme. Re value in the present paper ranges from 10000 to 60000, and the corresponding velocity ranges from 3.73 m/s to 22.4 m/s. The flow in the channel can be considered as incompressible flow. Besides the default quantities (such as continuity, energy and velocities), the pressure gradient per unit length of the channel and the area-averaged wall temperature are considered to judge the convergence of the computations. The computations are considered to be converged when the residues for continuity, energy, velocities, pressure gradient per unit length of the channel and the area-averaged wall temperature are less than 1×10^{-6}, 1×10^{-7}, 1×10^{-6}, 1×10^{-3}, and 1×10^{-3}, respectively.

Boundary Condition

In the ribbed rectangular channel, fully developed periodic velocity and temperature will obtained after x/D_h >3 as Han [3] reported. Under this condition, it is desirable to choose the smallest repetitive unit as the computational domain to minimize the computational cost. The Smallest Periodic Domain (SPD) contains one pitch of the ribs. Taking case 4 as an example, Fig. 4 shows details of the computational domain. The following boundary conditions are specified: (a) Uniform heat flux and no-slip boundary condition are applied at all walls of the rectangular channel. (b) Transitional periodic boundary condition is applied at the inlet and outlet: $\vec{U}(\vec{r})=\vec{U}(\vec{r}+\vec{L})$, $P(\vec{r})=P(\vec{r}+\vec{L})-\beta\left|\vec{L}\right|$, $T(\vec{r})=T(\vec{r}+\vec{L})-\dfrac{Q}{C_p\dot{m}}$, where $\vec{r}$ is the position vector and $\vec{L}$ is the periodic length vector of the domain. The computational method of dealing the fully developed periodic velocity and temperature was first introduced by Patankar[25].

Air enters the channel with a fully developed velocity and bulk temperature of 300 K.

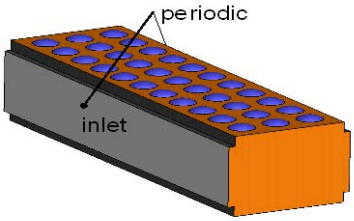

Fig. 4 Computational domain of case 4

Turbulence Model Selection and Validation

Prior to conducting the present numerical simulations, it is recognized that it is very important to select an appropriate turbulence model for the specified simulation. The main characteristics of the flow in rectangular channel with ribs/dimples/protrusions are separation, recirculation, and impingement. The agreement between the simulated results and experimental data is the main criterion for selecting a turbulence model. Three different turbulence models, i.e., the Realizable k-ε model, the RNG k-ε model, and the RSM model are chosen for simulation of the turbulent heat transfer of case 1. The enhanced wall treatment that resolves the sublayer region are used for all the turbulence models and the averaged Y^+ value is about 1.0. Fig. 5 compares the calculated Nusselt numbers and friction factor ratios with the data from Han[3]. From the figure, the Realizable k-ε model results agree better than the other two models. The maximum difference of *Nu* is 13%, and the maximum difference of friction factor ratio is 8.6%. Based on these calculations, the Realizable k-ε model is selected for all final computations. Also the numerical method of the present study is validated at the same time.

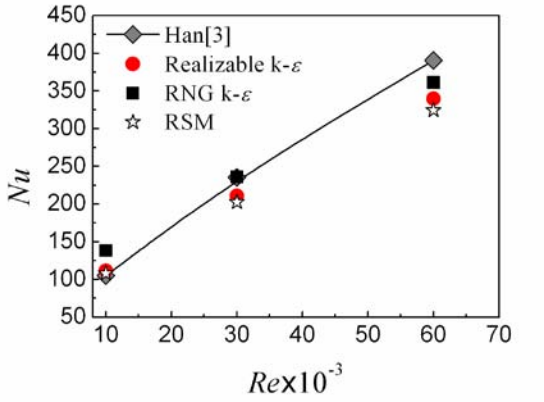

(a)

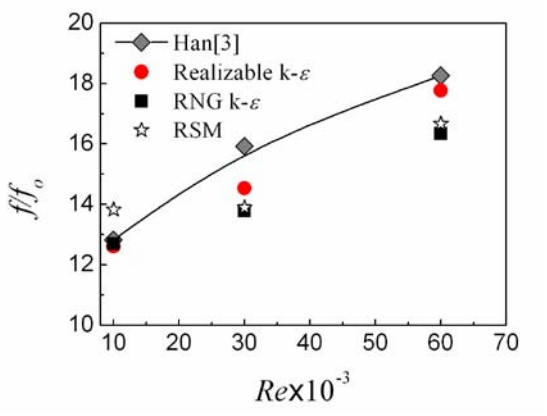

(b)

Fig. 5 Comparison of the calculated results with different turbulence model: (a) *Nu vs Re*; (b) f/f_0 *vs Re*

Grid Generation and Independence Study

The grid was generated with O-grid wrapped around the ribs, dimples and protrusions. An H-type grid was generated for the flow core. The averaged Y^+ value was below 1.0 for all cases. Taking case 4 as example, Fig. 6(a) shows the grid distribution, and Fig. 6(b) shows an amplified view of the grid around the ribs and dimples. Furthermore, a grid independence study is carried out for the present study. Taking case 4 with Re=10000 as example, five different grid systems are investigated. The grids are systematically refined with a constant grid refinement ratio 1.59. Table 2 summarizes the comparisons. The *Nu* and f/f_0 change by 1.3% and 0.5% from grid 4 to grid 5, respectively. Hence grid 4 is chosen. Grid independence is similarly established for the grids selected for the other cases.

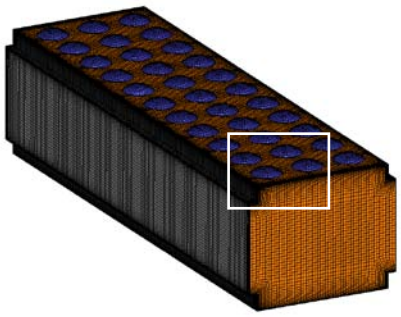

(a)

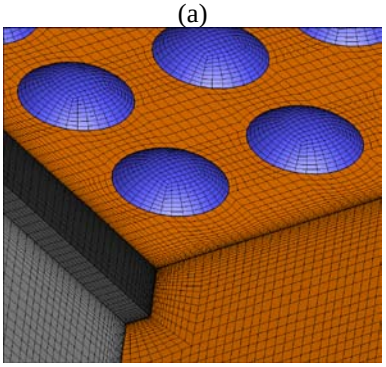

(b)

Fig. 6 Grid distribution of case 4: (a) overview of the grid distritution, and (b) amplified view of the grid distribution near the dimples and rib corner

Table 2 Grid independence study for case 4 at Re=10000

	grid1	grid2	grid3	grid4	grid5
	0.6	0.96	1.54	2.45	3.89
Nu	73.51	81.26	84.79	86.50	87.64
f/f_0	12.12	12.57	12.68	12.80	12.86
Nu %	16.12	7.28	3.25	1.3	Ref
f/f_0 %	5.76	2.32	1.47	0.5	Ref

Grid number unit: Million

Data Reduction

The Reynolds number in the present study is defined by

$$Re = \frac{\rho U_{m,in} D_h}{\mu} \tag{1}$$

where $U_{m,in}$ is the inlet average velocity. The hydraulic diameter D_h is given by

$$D_h = \frac{2WH}{W+H} \tag{2}$$

The local Nusselt number is described as

$$Nu_x = \frac{h_x D_h}{\lambda} \tag{3}$$

where λ is the thermal conductivity of air and the local heat transfer coefficient h_x is defined as

$$h_x = \frac{q''}{\Delta T_x} \tag{4}$$

where q'' represents the heat flux, and ΔT_x is the local temperature difference between the wall and the air which can be obtained as follows

$$\Delta T_x = T_{w,x} - T_x \tag{5}$$

where $T_{w,x}$ and T_x are the local wall and bulk mean temperatures, respectively.

The average Nusselt number for the channel can be calculated by

$$Nu = \left(\int Nu_x dA\right) / A \tag{6}$$

The Fanning friction factor f is defined as

$$f = -\frac{(\Delta p / L) D_h}{\frac{1}{2}\rho U_{m,in}^2} \tag{7}$$

where ΔP is the pressure drop and L is the streamwise channel length of the computational domain.

The thermal performance is

$$TP = \left(\frac{Nu}{Nu_0}\right) \cdot \left(\frac{f}{f_0}\right)^{-1/3} \tag{8}$$

The baseline Fanning friction factor f_0 and Nusselt number Nu_0 are given as

$$f_0 = 0.046 Re^{-0.2} \tag{9}$$

$$Nu_0 = 0.023 Re^{0.8} Pr^{0.4} \tag{10}$$

RESULTS AND DISCUSSION

Flow characteristics

Through an examination of all the cases, the flow characteristics are nearly the same at different *Re* for each

case. Taking *Re*=30000 as example, Fig. 7 shows the streamlines and Turbulent Kinetic Energy (TKE) contours at the center plane (*z*=0) near the ribbed/dimpled/protrusioned walls. Air flows from left side to right side in each case of Fig. 7. As known from the previous researches, the orthogonal ribs induce fundamentally two-dimensional flow phenomenon with flow separation and reattachment taking place between two consecutive ribs. Figure 7(a) shows that the calculated flow patterns agree well with the conceptual flow pattern of the ribbed channel. As the mainstream flow near the wall passes over the rib, it separates from the wall due to the rib. Then the mainstream flow reattaches to the wall (between two ribs). In case 2, the mainstream flow also separates when passing over the rib, and another recirculation occurs within the dimple. As a row of dimples located between two consecutive ribs, the mainstream flow reattachment occurs at the downstream edge of the dimple which is further downstream compared with the baseline case (case 1). In case 3, the mainstream flow separate from the wall and reattaches at the windward side of the protrusion and the recirculation is smaller compared with the baseline case. A small recirculation occurs at the leeward side of the protrusion. In case 4, there are three rows of dimples located between two ribs and each dimple contains a recirculation. The mainstream flow reattaches at the downstream edge of the dimples in the second row. In case 5, the mainstream flow separates from the wall and reattaches at the windward side of the prostrusions in the second row. Between the rib and the protrusions of the first row, the first row and the second row, the second row and the third, the third row and the next rib, small recirculation occurs.

The TKE levels give a good indication of vortices generation, flow mixing and energy transfer. TKE contours at the center plane (*z*=0) are also presented in Fig. 7. Higher levels of TKE are observed in the separated shear layer near the ribbed/dimpled/protrusioned wall where the mainstream flow and the recirculation interact. Thus, the relatively hot fluid near the wall is continuously mixing with the cooler core fluid. This mixing increases the heat transfer from the channel wall.

Local Nusselt number distribution

The local Nussult number distribution patterns are also nearly the same at different *Re* for each case. Taking *Re*=30000 as example, Fig. 8 shows the local Nusselt number distributions of all five cases on the channel wall with ribs/dimples/protrusions. Air flows from left side to right side in each case of Fig. 8. The circle lines identify edges of individual dimples/protrusions. In case 1, higher local Nusselt number values are located at the rib surfaces and the walls between the ribs where the mainstream flow reattaches. There is a relative low local Nusselt number region just downstream of the rib for all the cases. It is due to a relatively hot cell being trapped in the area of recirculation. For case 2, higher local Nusselt number are located near the downstream edge of the dimples where the mainstream flow reattaches, and relative low local Nusselt number are located in the upstream portion of the dimple where recirculation occurs. For case 3, higher local Nusselt number are located at upstream portion of the protrusion due to the mainstream flow reattaches and impinges on the protrusions. Relatively low local Nusselt number occurs at the leeward side where small recirculation presents. For case 4, relatively higher local Nusselt number are located near downstream edge of the dimples in the first two rows. As mainstream flow does not reattach at the downstream edge of the dimples in the third row, local Nusselt number values are relative lower near the region of the third row. For case 5, higher local Nusselt number are locate at the upstream portion of the protrusions in the downstream two rows. The first row protrusions provide relative lower local Nusselt number value because the recirculations nearly cover all the aera of first row. It can be concluded that the mainstream flow reattachment serves to increase the heat transfer and the recirculation leads to decrease in the heat transfer.

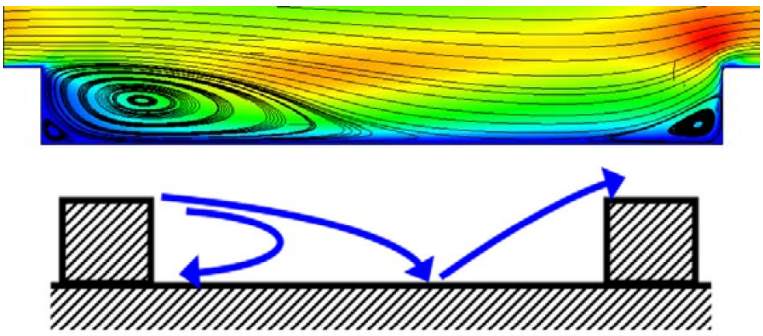

(a) case 1(up) and conceptual view from Han[7](down)

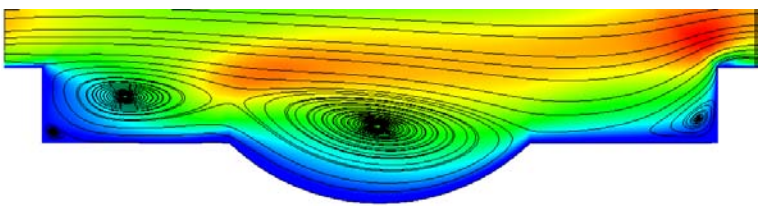

(b) case 2

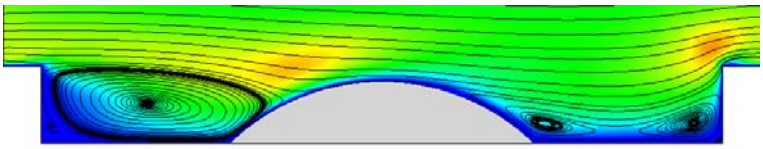

(c) case 3

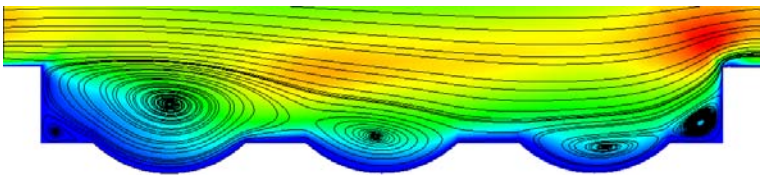

(d) case 4

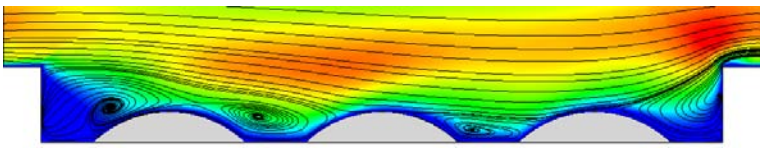

(e) case 5

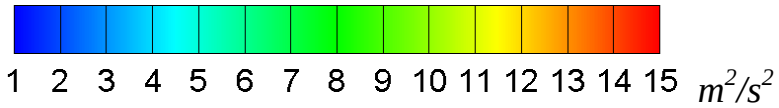

Fig. 7 Streamlines and TKE contours at the center plane (z=0) near the ribbed/dimpled/protrusioned wall

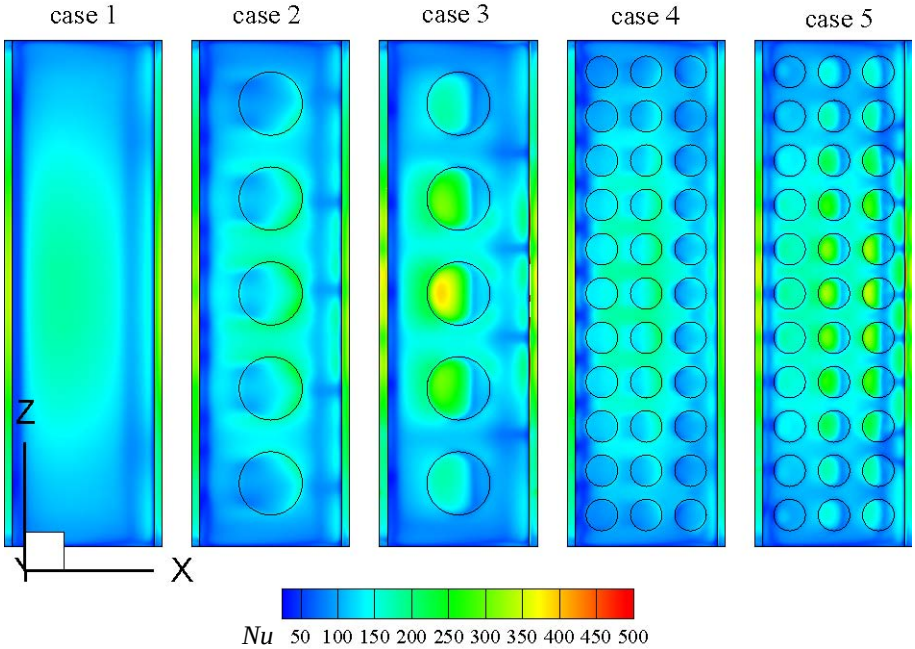

Fig. 8 Local Nusselt number distribution at Re=30000

Average Nusselt number and friction characteristics

Figure 9(a) compares normalized average Nusselt number of different cases at different Reynolds numbers of the roughened walls. As Fig. 9(a) presents, Nu/Nu_0 in each case decreases as Reynolds number increases. Three other features may be noted. First, the rib+protrusion cases provide larger Nu/Nu_0 than the rib+dimple cases. It can be observed that the Nu/Nu_0 value of case 5 is about 17%, 12%, 7% larger than that of the baseline case for Re=10000, Re=30000 and Re=60000, respectively. Second, the three row dimple arrangement (protrusion arrangement) provide larger Nu/Nu_0 than that of the one row dimple arrangement (protrusion arrangement). Third, Nu/Nu_0 value of the one row dimple arrangement case is smaller than the baseline case at Re=60000.

Figure 9(b) shows the variations of normalized friction factor with Reynolds numbers. The main feature is that f/f_0 increases as Re increases in each case. The rib+dimple cases

(case 2 and case 4) lead to larger f/f_0 than the baseline case and the rib+protrusion cases (case 3 and case 5) provide smaller f/f_0 than the baseline case. It is to be noted that within the range of Reynolds number compared (from 10000 to 60000), the f/f_0 value is about 10% and 12 % lower than that of the baseline case for case 5 and case 3.

Figure 10 compares the thermal performance (*TP*) of all the cases. By carefully examining the results, it can be noted that the thermal performance variation trend is: (1) The rib+protrusion cases perform much better than the rib+dimple cases; (2) The *TP* value of the rib+dimple cases are nearly the same to the baseline case. The thermal performance of case 5 is about 16% higher than that of the baseline case, and the thermal performance of case 3 is about 14% higher than the baseline case.

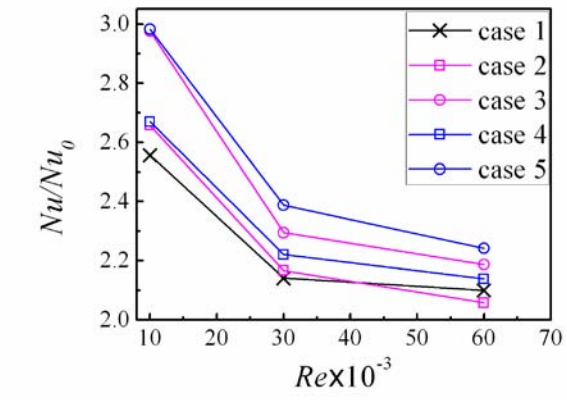

(a)

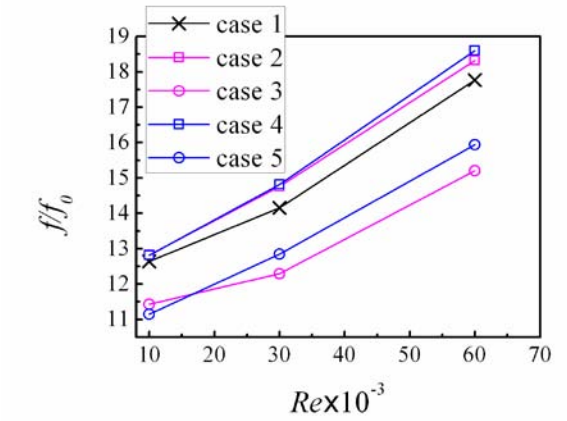

(b)

Fig. 9. Heat transfer and friction characteristics: (a) Nu/Nu_0 variations with Reynolds number, and (b) f/f_0 variations with Reynolds number

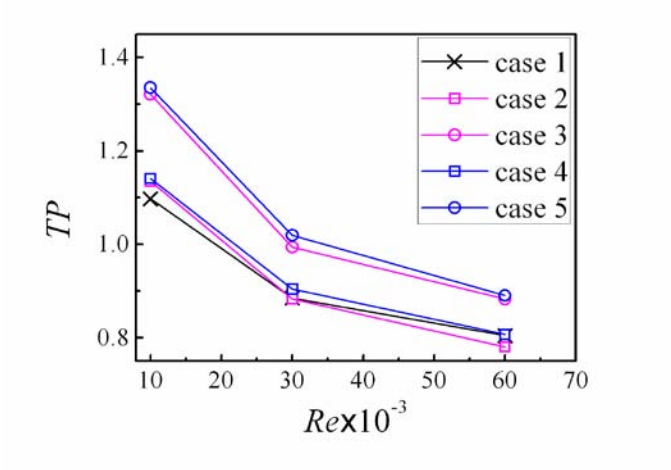

Fig. 10 Thermal performance variations with Reynolds number

CONCLUSION

Flow characteristics and heat transfer performances were studied in a rectangular channel (AR=4) with rib+dimple and rib+protrusion with Reynolds number within the range of 10000 to 60000. Based on the present study, it can be concluded that rib+protrusion technique in rectangular channel has the potential to provide heat transfer enhancement with low pressure penalty. The following findings/conclusions can be drawn from the present work in detail:

1. The main flow characteristics of the rib/dimple/protrusion roughened channel is the mainstream flow separation, reattachment, and recirculation. The flow reattachment serves to increase the heat transfer, and the recirculation leads to heat transfer reduction. The ribs/dimples/protrusions located on the channel walls also increase the mixing of the flow and increase the heat transfer.
2. The rib+dimple cases provide both minor increase in Nu/Nu_0 and f/f_0. As a result, the thermal performance of the rib+dimple cases is nearly the same to the baseline case.
3. Within the Reynolds number range studied, the Nu/Nu_0 values of the three row rib+protrusion case is 17% ~ 7% higher than that of the baseline case, and the decrease in f/f_0 is about 10%. The thermal performance of the three row rib+protrusion case is about 16% higher than that of the baseline case.
4. Within the Reynolds number range studied, the Nu/Nu_0 values of the one row rib+protrusion case is about 9% higher than that of the baseline case, and the decrease in f/f_0 is about 12%. The thermal performance of the three row rib+protrusion case is about 14% higher than that of the baseline case.

ACKNOWLEDGMENTS

The research work was sponsored by Hi-Tech Research and Development Program of China (Grant No. 2009AA04Z102), National Natural Science Foundation of China (Grant No. 10602044) and Program for New Century Excellent Talents in University of China (Grant No. NCET-07-0682).

NOMENCLATURE

AR	=	aspect ratio
D	=	dimple/protrusion print diameter (m)
D_h	=	hydraulic diameter (m)
f	=	Fanning friction factor
H	=	channel height (m)
h	=	heat transfer coefficient (W m^{-2} K^{-1})
L	=	steamwise length (m)
Nu	=	Nusselt number
P	=	spanwise pitch of the ribs (m)
P_d	=	spanwise pitch of the dimples (m)
q''	=	heat flux (W m^{-2})
Re	=	Renolds number
S	=	streamwise pitch (m)
T	=	temperature (K)
TP	=	thermal performance
U	=	velocity (m s^{-1})
W	=	channel width (m)
ΔP	=	pressure drop (Pa)
ΔT	=	mean temperature difference (K)

Greek symbols

δ	=	dimple/protrusion depth (m)
λ	=	thermal conductivity (W m^{-1} K^{-1})
ρ	=	density (kg m^{-3})

Subscripts

in	=	inlet
m	=	mass flow average
out	=	outlet
w	=	wall

REFERENCES

[1] J.C. Han, L.R. Glicksmana and W.M. Rohsenow, 1978, ‘‘An investigation of heat transfer and friction for rib-roughened surfaces,’’ International Journal of Heat and Mass Transfer, 21(8), pp. 1143-1156.

[2] J.C. Han, 1984, ‘‘Heat transfer and friction in channels with two opposite rib roughened walls,’’ ASME J. Heat Transfer, 106, pp. 774–781.

[3] J.C. Han, 1988, ‘‘Heat transfer and friction characteristics in rectangular channels with rib turbulators,’’ ASME J. Heat Transfer 110, pp. 321–328.

[4] J.C. Han, and J.S. Park, 1988, ‘‘Developing heat transfer in rectangular channels with rib turbulators,’’ Int. J. Heat Mass Transfer, 31(xx), pp. 183–195.

[5] J.S. Park, J.C. Han, Y. Huang, and S. Ou, 1992, ‘‘Heat transfer performance comparisons of five different rectangular channels with parallel angled ribs,’’ Int. J. Heat Mass Transfer 35 (11) , pp. 2891–2903.

[6] G.S. Azad, J.C. Han, H.K. Moon, B. Glezer, 2002, ‘‘Heat transfer in a two-pass rectangular rotating channel with 45-deg angled rib turbulators,’’ ASME J. Turbomachinery 124, pp. 251–259.

[7] Michael Huh, Yao-Hsein Liu, Je-Chin Han, 2010, ‘‘Effect of rib height on heat transfer in a two pass rectangular channel (AR = 1:4) with a sharp entrance at high rotation numbers,’’ International Journal of Heat and Mass Transfer, 52, pp. 4635–4649.

[8] P. M. Ligrani, M. M. Oliveira and T. Blaskovich, 2003, ‘‘Comparison of Heat Augmentation Techniques,’’ AIAA Journal, 41 (3), pp. 337-362.

[9] V.N. Afanasyev, Y.P. Chudnovsky, A.I. Leontiev, and P.S. Roganov, 1993, ‘‘Turbulent Flow Friction and Heat Transfer Characteristics for Spherical Cavities on a Flat Plate,’’ Experimental Thermal and Fluid Science, 7, pp. 1–8.

[10] H.K. Moon, T. O’Connel, and B. Glezer, 2000, ‘‘Channel Height Effect on Heat Transfer and Friction in a Dimple Passage,’’ Journal of Engineering for Gas Turbines and Power, 122, pp. 307–313.

[11] P.M. Ligrani, J.L. Harrison, G. I. Mahmmod, and M. L. Hill, 2001, ‘‘Flow structure due to dimple depressions on a channel surface,’’ Physics of Fluid, 13(11) , pp. 3442-3451.

[12] G.I. Mahmood and P.M. Ligrani, 2002, ‘‘Heat Transfer in a Dimpled Channel: Combined Influences of Aspect Ratio, Temperature Ratio, Reynolds Number, and Flow Structure,’’ International Journal of Heat and Mass Transfer, 45, pp. 2011–2020.

[13] P.M. Ligrani, G.I. Mahmood, J.L. Harrison, C. M. Clayton, and D.L. Nelson, 2001, ‘‘Flow Structure and Local Nusselt Number Variation in a Channel With Dimples and Protrusions on Opposite Walls,’’ International Journal of Heat and Mass Transfer, 44 , pp. 4413–4425.

[14] S.Y. Won, Q. Zhang, and P.M. Ligrani, 2005, ‘‘Comparisons of Flow Structure Above Dimpled Surfaces With Different Dimple Depths in a Channel,’’ Physics of Fluids, 17 , pp. 045105.

[15] N.K. Burgess and P. M. Ligrani, 2005, ‘‘Effects of Dimple Depth on Channel Nusselt Numbers and Friction Factors,’’ ASME Journal of Heat Transfer, 127, pp. 839–847.

[16] P.M. Ligrani, N. K. Burgess, and S. Y. Won, 2005, ‘‘Nusselt Numbers and Flow Structure on and Above a Shallow Dimpled Surface Within a Channel Including Effects of Inlet Turbulence Intensity Level,’’ ASME Journal of Turbomachaniery, 127, pp. 321–330.

[17] E. Small, S.M. Sadeghipour, and M. Asheghi, 2006, ‘‘Heat Sinks With Enhanced Heat Transfer Capability for Electronic Cooling Applications,’’ ASME J. Electronic Packaging, 128, pp. 285–290.

[18] N. Xiao, Q. Zhang, P.M. Ligrani, and R. Mongia, 2009, ‘‘Thermal performance of dimpled surfaces in laminar flows, International Journal of Heat and Mass Transfer,’’ 52, pp. 2009–2017.

[19] S.A. Isaev, A.I. Leont'ev, D.P. Frolov, and V.B. Kharchenko, 1998, ‘‘Identification of self-organizing

structures by the numerical simulation of laminar threedimensional flow around a crater on a plane by a flow of viscous incompressible fluid,'' Technical Physics Letters, 24 (3), pp. 209-211.
[20] J. Park, P.R. Desam, and P.M. Ligrani, 2004, ''Numerical predictions of flow structure above a dimpled surface in a channel,'' Numerical Heat Transfer A, 45 (1) , pp. 1-20.
[21] Z.Y. Wang, K.S. YEO, and B.C. KHOO, 2006, ''DNS of low Reynolds number turbulent flows in dimpled channels,'' Journal of Turbulence, 7 (37) , pp. 1–31.
[22] X.J. Wei, Y.K. Joshi, and P.M. Ligrani, 2007, ''Numerical Simulation of Laminar Flow and Heat Transfer Inside a Micro-Channel With One Dimpled Wall,'' ASME Journal of Electronic Packaging, 129 , pp. 63-70.
[23] M.A Elyyan and D.K. Tafti, 2009, ''Flow and Heat Transfer Characteristics of Dimpled Multilouvered Fins,'' Journal of Enhanced Heat Transfer, 16 , pp. 43-60.
[24] M.A. Elyyan and D.K. Tafti, 2010, ''Effect of Coriolis forces in a rotating channel with dimples and protrusions,'' International Journal of Heat and Fluid Flow, 31, pp. 1-18.
[25] Patankar S.V., Lui C.H., Sparrow E.M., 1977, ''Fully developed flow and heat transfer in ducts having streamwise-periodic variations of cross-sectional aera,'' ASME Journal of Heat transfer, 99, pp. 323-357.